Published in final edited form as:
J Immunol Methods. 2010 August 31; 360(1-2): 167–172. doi:10.1016/j.jim.2010.06.016.

Functional lymphatic imaging in tumor-bearing mice

Sunkuk Kwon and **Eva M. Sevick-Muraca**[1]
Center for Molecular Imaging, The Brown Foundation Institute of Molecular Medicine The University of Texas Health Science Center, Houston, TX

Abstract

The lymphatic system provides a route for dissemination of metastatic cancer cells. Yet to date transient changes in lymphatic drainage pathways and function as a result of tumor growth and metastasis has not been completely elucidated. Herein, we non-invasively imaged functional and architectural lymphatic changes in mice with regional, palpable lymph node (LN) involvement using dynamic near-infrared (NIR) fluorescence imaging with intradermal injection of indocyanine green (ICG) to both tumor-free mice and mice bearing C6/LacZ rat glioma tumors in the tail or hindlimb. We found that lymphatic drainage pathways were transiently altered and the contractile function of regional conducting lymphatic vessels was reduced or lost with progressive disease. Therefore, transient changes in the regional lymphatic architecture and function occur with progressive disease, can be imaged using NIR fluorescence, and may provide a new method to stage disease.

Keywords

contractile lymphatic function; functional lymphatic imaging; near-infrared fluorescence imaging; tumor metastasis

1. Introduction

The lymphatic system plays an important role in immune surveillance and fluid homeostasis. In addition, the lymphatic system provides a major route of cancer cell dissemination from the primary lesion site to regional draining lymph nodes (LNs) (Stacker et al., 2002). In preclinical studies, lymph sinus remodeling/dilation along with LN lymphangiogenesis in sentinel LNs (SLNs) (Harrell et al., 2007; Qian et al., 2006) and increased afferent lymph flow to tumor-draining LNs (Harrell et al., 2007; Ruddell et al., 2008) have been shown to occur prior to LN metastasis. Therefore, non-invasive functional imaging of changes in lymphatic function and architecture may allow early identification of metastatic potential and lymphatic involvement. Yet to date, there is no translatable method to directly and longitudinally monitor changes in lymphatic structure and function with progressive disease or in response to therapy. Most importantly, there are no established clinical imaging techniques with sufficient resolution to detect the remodeling of the lymphatic vasculature

[1]To whom correspondence should be directed, Center for Molecular Imaging, The Brown Foundation of Molecular Medicine, The University of Texas Health Science Center, 1825 Pressler Street, SRB 330A, Houston, Texas 77030; phone: 713-500-3561; fax: 713-500-0319; eva.sevick@uth.tmc.edu.

and the change in lymphatic function that may occur prior to and as a result of LN metastasis (Sharma et al., 2008).

Near-infrared (NIR) fluorescent dyes, that are excited and emit in the 750 to 950 nm wavelength range, have the opportunity to assess lymphatic function due to lack of tissue autofluorescence as well as due to low tissue absorption and scattering that results in increased tissue penetration depth. Recently, we have developed near-infrared (NIR) fluorescence imaging to assess lymphatic function and architecture in both mice (Kwon and Sevick-Muraca, 2007) and humans (Rasmussen et al., 2009; Sevick-Muraca et al., 2008). The technique is based upon (i) the illumination of dim, tissue penetrating NIR excitation light on tissue surfaces to excite a lymphotropic fluorophore taken up within lymphatic structures following intradermal (i.d.) administration, and (ii) the selective collection of NIR fluorescence using sub-second acquisition times in order to provide temporal resolution of lymphatic function. Herein we show alteration in the lymphatic architecture and function as a result of LN metastasis in an animal model of cancer progression. If translated, the imaging approach could provide a new method for diagnostic LN staging and evaluation of therapeutic agents that target lymphangiogenesis as a means to inhibit metastasis.

2. Materials and Methods

2.1 Animals

Four to six weeks old female Balb/c nude mice (Charles River, Wilmington, MA) were housed and fed sterilized pelleted food and sterilized water. Animals were maintained in a pathogen-free mouse facility accredited by the American Association for Laboratory Animal Care. All experiments were performed in accordance with the guidelines of the Institutional Animal Care and Use Committee. Animal experiments were approved by University of Texas Health Science Center Institutional Animal Care and Usage Committee in accordance with NIH guidelines.

2.2. Cell line

The rat glioma cell line C6/LacZ was purchased from ATCC and provided by Dr. Bagri (Genentech Inc., San Francisco, CA). It has been shown that subcutaneous implantation of C6 cells in nude mice resulted in development of LN and lung metastases via the lymphatic system (Schreiber et al., 2002; Caunt et al., 2008). In addition, C6 cells minimally express neuropilin (Nrp)-2 on their surface as well as vascular endothelial growth factor (VEGF)-C (Caunt et al. 2008). Therefore, this cell line may be suitable for monitoring *in vivo* response to potential anti-metastatic cancer therapy that targets pro-lymphangiogenic signaling from Nrp-2 and VEGFR-3. Tumor cells were cultured in DMEM (GIBCO) supplemented with 10% FBS. All cells were maintained at 37 °C in a 5% CO_2, 95% humidity incubator. Cells (500,000 per animal) were implanted intradermally in one of two distinct sites: in the right hindlimb or in the tail at 1 to 2 cm caudal to the rectum in mice. Nodal involvement was assessed from gentle palpation of ischial, inguinal, and axillary LNs in these longitudinal imaging studies and hard and enlarged LNs were assumed to be metastatic.

2.3. In vivo NIR lymphatic imaging

Nine tail-tumor-bearing mice were imaged at 3 weeks post implantation (p.i.) and 10 hindlimb-tumor-bearing mice were imaged at 2 and 3 weeks p.i.. In addition, 7 non-tumor-bearing mice as control for a tail tumor model and 6 tumor-free mice as control for a hindlimb tumor model were also imaged. Mice were anesthetized with isofluorane and maintained at 37 °C on a warming pad. Previously, we showed lymphatic function and drainage pathway in normal mice after i.d. injection of 2-10ul of 1.3mM of ICG into the dorsal aspect of the foot and the tail (Kwon and Sevick-Muraca, 2007). In this study, a

volume of 10 μl of 645 μM of IC-Green (Akorn, Inc. Buffalo Grove, IL) dissolved in mixture of distilled water and 0.9 % Sodium Chloride in a volume ratio of 1:9 was injected intradermally either (i) 2-3 cm away from the tip of the tail for a tail tumor model or (ii) at the dorsal base of the tail the hindlimb tumor model. The i.d. delivery was conducted using with 31 gauge needles (BD Ultra-Fine™ II Short Needle, Becton and Dickinson Medical, Franklin, NJ) and evident by high interstitial pressure during the injections.

Fluorescence images were acquired immediately before and for up to 30 min after i.d. injection using a custom-built NIR fluorescence imaging system. In the previous study (Kwon and Sevick-Muraca, 2007), the camera exposure time was 100 ms and the power of a laser diode was 80mW. In this study, a field of view (FOV) was illuminated with 785 nm light from a laser diode (500 mW, Intense Ltd., North Brunswick, NJ) outfitted with a convex lens and diffuser to create a uniform excitation field. The fluorescence was collected through holographic (model HNPF-785.0-2.0, Kaiser Optical Systems Inc., Ann Arbor, MI) and interference (Image quality, Andover Corp., Salem, NH, model 830.0-2.0) filters placed prior to a 28 mm Nikon lens (Nikon, Japan). A macrolens (Infinity K2/SC video lens, Edmund Optics Inc., Barrington, NJ) was also used to zoom in on a specific area in fluorescent lymphatic vessels. The images were finally captured by an electron-multiplying CCD camera (EMCCD, PhotonMax, Tucson, AZ) with 200 ms integration time for dynamic imaging and 800 ms for static imaging. For acquisition of white-light images, the optical filters were removed and a low-power lamp illuminated the subject. Image acquisition was accomplished by V++ software (Digital Optics, Aukland, New Zealand).

2.4. Data analysis

The data were analyzed with Matlab (The MathWorks, Inc., Natick, MA) and ImageJ (National Institutes of Health, Bethesda, MD). To reveal contractile activity resulting in propulsive lymph flow, the same size of fixed regions of interest (ROIs) in fluorescent lymphatic vessels were defined on fluorescence images. The averaged fluorescence intensity within each ROI in each fluorescence image was normalized by the maximum average value and then plotted as a function of imaging time over 5 min at 10 min after i.d. injection for a tail tumor model and at 5 min post injection of ICG for a hindlimb tumor model. The number of “pulses” of ICG-laden lymph is an indication of lymphatic contractile activity and termed as “contractions.” Statistical analysis was performed with SPSS 12.0.1 statistical program (SPSS, Inc., Chicago, Illinois). The data were analyzed using Student t-test and the differences were considered significant at $p < 0.05$.

3. Results and Discussion

3.1. Tail tumor model

Figure 1 shows an example of white light and fluorescence images of a tail in tumor-free and tumor-bearing mice 15 min after i.d. injection of ICG. Fluorescent images in tumor-free mice as depicted in Figure 1B show (i) the circumferential honeycomb lymphatic structure near the injection site, (ii) well-defined fluorescent collecting lymphatic vessels, and (iii) the draining ischial LN. The draining honeycomb structure has also been reported by others (Kwon and Sevick-Muraca, 2007;Leu et al., 1994). In tumor-bearing mice, abnormal lymphatic drainage to the ventral region of a tail-tumor-bearing mouse was also detected as denoted by arrow head in Figure 1D, due presumably to the complete tumor blockage of lymphatic drainage to the ischial LNs. Therefore, ischial LNs were not visualized from fluorescent imaging. Magnified fluorescent images in another tail-tumor-bearing mouse reveal that the collecting lymphatic vessels are uncharacteristically tortuous and dilated as denoted by small arrows in Figure 1E as compared to those in tumor-free mice (supplemental Figure 2). In agreement with other reports (Leu et al., 2000), uptake or

drainage of fluorophore was never observed in the lymphatic capillaries in the skin above the tumor in all tail-tumor-bearing mice. Figure 1F shows dynamic changes of fluorescent intensities as a function of time in the ROI 1 of the normal mouse tail depicted in Figure 1B, demonstrating propulsive lymphatic function and drainage of ICG from the injection site to the ischial LN. In contrast, loss or reduction of lymph propulsion was observed in the tail-tumor-bearing mice as depicted in Figure 1G, where the number of contractions in tumor-free mice is significantly higher than that observed in tumor-bearing mice. The results are consistent with reduced function of the lymphatic collecting vessels and enhanced transiting through the honeycomb lymphatic vessels away from the primary tumor.

3.2. Hindlimb tumor model

The right hindlimb of tumor-bearing and tumor-free mice were also imaged immediately before and after i.d. injection of ICG to the base of the mouse tail. As shown in Figure 2, the fluorescent lymphatic plexus was seen in the dorsal or ventral views of the tumor-free mouse limb and drained to the inguinal LNs. Fluorescence in the liver as denoted by double arrows was also observed. The signal from the liver is expected as a route of clearance of ICG from the body. In addition, Figure 2B shows the internodal collecting lymphatic vessels draining into the axillary LNs (which are more clearly shown in the supplemental Figure 1). These lymphatic vessels are typical in both lateral sides of tumor-free mice. Figure 2C shows normalized fluorescent intensity profiles in the ROI 1 shown in Figure 2A, demonstrating propulsive lymphatic function in a collecting lymphatic vessel in a tumor-free mouse.

In contrast, the hindlimb-tumor-bearing mice presented abnormal lymphatic drainage patterns and loss or reduction of contractile function with increasing tumor involvement first to the inguinal and subsequently to the axillary LNs. For example, Figures 3A and 3B show that the internodal collecting vessels efferent to the inguinal LN and afferent to the axillary LN were not functional as evident from lack of ICG fluorescence. Instead, re-routing of lymphatic drainage was visualized as denoted by arrow. Interestingly, this mouse showed greater tumor invasion of the axillary LN than the inguinal LN at 3 weeks p.i. and the abnormal lymphatic drainage pattern persisted. At 2 weeks p.i., 3 out of 10 animals displayed palpable inguinal LN metastasis, while none exhibited palpable axillary LN metastasis. Of the 3 animals with palpable inguinal LN metastasis, one displayed abnormal lymphatic patterning and none showed contractile lymphatic function. Figures 3C and 3D show that the inguinal LN generally became enlarged and the lymphatic vessels became tortuous and leaky as indicated by the bright spots. In addition, lymphatic vessels that transported ICG circumvented the primary tumor, which is another common feature observed in the hindlimb tumor model.

At 3 weeks p.i., only one animal retained normal lymphatic patterning and exhibited contractile lymphatic function; this animal did not possess palpable LN metastases. In contrast, the palpable inguinal LN metastasis was detected in 9 out of 10 mice, five of which also showed the axillary LN metastasis. All 5 mice with palpable inguinal and axillary LN metastases showed further alteration of lymphatic drainage directly to the brachial LN or to the contralateral left axillary LN with diffuse dye patterns along tortuous and dilated lymphatic vessels. An example of abnormal lymphatic drainage during tumor progression is shown in Figures 3E and 3F. Figures 3E and 3F provide the white light and fluorescent images of the mouse depicted in Figures 3C and 3D but taken one week later. New tortuous and dilated lymphatic vessels were fluorescently stained and partially drained to the inguinal LN basin, yet the majority of the fluorescent lymphatic vessels circumvented both the primary tumor and the inguinal LN and reached the brachial LN as depicted by double arrow in Figure 3F. Supplemental movie #1 shows that dye moves to the tumor periphery immediately after injection and drains back to the injection site within a few seconds after

i.d. injection. Figures 3G and 3H represent the final example of a mouse with massive inguinal and axillary LN metastases at 3 weeks p.i., depicting the extensive, stained lymphatic network of tortuous and dilated lymphatic vessels, which was not observed in tumor-free mice. In addition, ICG-labeled lymph drained across the midline of the animal body and thus to the left axillary LN. The inset of Figure 3H represents a magnified fluorescent image of a rectangle in Figure 3H showing diffused dye patterns. Table 1 shows the summary of the LN status and lymphatic drainage patterns in mice with a hindlimb tumor at 2 and 3 weeks p.i..

4. Conclusion

Extensive tumor invasion of draining LNs can alter or completely block normal lymphatic fluid passage, leading to changes of lymphatic drainage pathways and altered integrity of the lymphatic vasculature that can aid in the formation of local and secondary metastases. It has been postulated that tumor blockage of lymphatic drainage prevents inflow of lymph fluid into the draining LNs thus resulting in change of normal lymphatic drainage pathways (Leijte et al., 2009). Although palpation may be an inaccurate technique tostage lymph node involvement in this study, it is the clinical standard as intraoperative palpation of suspicious LNs may reduce false negative rates of sentinel LNs in patients with breast cancer (Choi et al., 2008). In fact, all suspicious metastatic LNs at 2 and 3 weeks post implantation were swollen and hard. For longitudinal imaging, tissue samples could not be collected at 2 weeks p.i. and hence palpation was the measure utilized. Nonetheless, based upon our technical studies of NIR fluorescence imaging presented herein, *in vivo* NIR lymphatic imaging demonstrates transient changes in overall lymphatic function and architecture in response to tumor growth and metastasis. In these studies, it is noteworthy that the lymphatic flow indicated by ICG may not mimic migration of tumor cells to the draining basins, since ICG was intradermally injected into distant sites from the primary tumor (i.e., ~3cm from the tip of the tail in a tail tumor model and the base of the tail in a hindlimb tumor model). Yet it has been reported that all SLNs detected with injection of a mapping agent at the tumor site in melanoma patients were also visible with distant injection (Rettenbacher et al., 2001). Therefore, functional NIR lymphatic imaging may potentially provide a better prognostic means to determine LN metastasis on the basis of architectural and functional changes. Whether images of either tumor model (i.e., tail and hindlimb tumor models) demonstrate lymphangiogenesis, the normal biological processes of co-opting otherwise non-functional lymphatic vessels in response to edema or elevated interstitial pressures, or a combination of both, requires further longitudinal imaging studies to understand the temporal relationship of key signaling molecules and receptors, cancer status of draining LNs, and alterations in lymphatic function and structure visualized in these feasibility studies.

In other studies from our laboratory (Rasmussen et al., 2009), we have employed NIR fluorescence imaging to visualize lymphatic function and architecture in normal human subjects as well as aberrant dysfunction and architecture in subjects who have undergone nodal staging surgery and/or suffer from lymphatic disorders. Whether the functional and architectural changes reported herein and in our previously reported human studies occur in the regional lymphatics of patients with metastatic disease remains to be answered in ongoing work. Nonetheless, the animal work presented herein provides preclinical evidence for the use of NIR fluorescence imaging for evaluating the lymphatic response for possible clinical cancer diagnostics as well as for further study to understand the role of the lymphatics in cancer progression and immune responses to tumors.

Supplementary Material

Refer to Web version on PubMed Central for supplementary material.

Acknowledgments

This work was supported in parts by Genentech, Inc. and R01 CA128919-01 (EMS). The authors acknowledge the discussions with Anil Bagri on the tail-tumor model and the assistance of Holly Robinson and John Rasmussen.

Abbreviations

ALD	abnormal lymphatic drainage
ICG	indocyanine green
i.d.	intradermal
LN	lymph node
LNM	LN metastasis
NIR	near-infrared
NLD	normal lymphatic drainage
p.i.	post implantation

References

Caunt M, Mak J, Liang WC, Stawicki S, Pan Q, Tong RK, Kowalski J, Ho C, Reslan HB, Ross J, Berry L, Kasman I, Zlot C, Cheng Z, Le Couter J, Filvaroff EH, Plowman G, Peale F, French D, Carano R, Koch AW, Wu Y, Watts RJ, Tessier-Lavigne M, Bagri A. Blocking neuropilin-2 function inhibits tumor cell metastasis. Cancer cell. 2008; 13:331. [PubMed: 18394556]

Choi YJ, Kim JH, Nam SJ, Ko YH, Yang JH. Intraoperative identification of suspicious palpable lymph nodes as an integral part of sentinel node biopsy in patients with breast cancer. Surg Today. 2008; 38:390. [PubMed: 18560959]

Harrell MI, Iritani BM, Ruddell A. Tumor-induced sentinel lymph node lymphangiogenesis and increased lymph flow precede melanoma metastasis. Am. J. Pathol. 2007; 170:774. [PubMed: 17255343]

Kwon S, Sevick-Muraca EM. Noninvasive quantitative imaging of lymph function in mice. Lymphat. Res. Biol. 2007; 5:219. [PubMed: 18370912]

Leijte JA, van der Ploeg IM, Valdes Olmos RA, Nieweg OE, Horenblas S. Visualization of tumor blockage and rerouting of lymphatic drainage in penile cancer patients by use of SPECT/CT. J. Nucl. Med. 2009; 50:364. [PubMed: 19223404]

Leu AJ, Berk DA, Lymboussaki A, Alitalo K, Jain RK. Absence of functional lymphatics within a murine sarcoma: a molecular and functional evaluation. Cancer Res. 2000; 60:4324. [PubMed: 10969769]

Leu AJ, Berk DA, Yuan F, Jain RK. Flow velocity in the superficial lymphatic network of the mouse tail. Am. J. Physiol. Heart .Circ. Physiol. 1994; 267:H1507.

Qian CN, Berghuis B, Tsarfaty G, Bruch M, Kort EJ, Ditlev J, Tsarfaty I, Hudson E, Jackson DG, Petillo D, Chen J, Resau JH, Teh BT. Preparing the “soil”: the primary tumor induces vasculature reorganization in the sentinel lymph node before the arrival of metastatic cancer cells. Cancer Res. 2006; 66:10365. [PubMed: 17062557]

Rasmussen JC, Tan IC, Marshall MV, Fife CE, Sevick-Muraca EM. Lymphatic imaging in humans with near-infrared fluorescence. Curr. Opin. Biotechnol. 2009; 20:74. [PubMed: 19233639]

Rettenbacher L, Koller J, Kassmann H, Holzmannhofer J, Rettenbacher T, Galvan G. Reproducibility of lymphoscintigraphy in cutaneous melanoma: can we accurately detect the sentinel lymph node by expanding the tracer injection distance from the tumor site? J. Nucl. Med. 2001; 42:424. [PubMed: 11337518]

Ruddell A, Harrell MI, Minoshima S, Maravilla KR, Iritani BM, White SW, Partridge SC. Dynamic contrast-enhanced magnetic resonance imaging of tumor-induced lymph flow. Neoplasia. 2008; 10:706. [PubMed: 18592009]

Schreiber S, Gross S, Brandis A, Harmelin A, Rosenbach-Belkin V, Scherz A, Salomon Y. Local photodynamic therapy (PCT) of rat c6 glioma xenografts with Pd-Bacteriopheophorbide leads to decreased metastases and increase of animal cure compared with surgery. Int. J. Cancer. 2002; 99:279. [PubMed: 11979445]

Sevick-Muraca EM, Sharma R, Rasmussen JC, Marshall MV, Wendt JA, Pham HQ, Bonefas E, Houston JP, Sampath L, Adams KE, Blanchard DK, Fisher RE, Chiang SB, Elledge R, Mawad ME. Imaging of lymph flow in breast cancer patients after microdose administration of a near-infrared fluorophore: feasibility study. Radiology. 2008; 246:734. [PubMed: 18223125]

Sharma R, Wendt JA, Rasmussen JC, Adams KE, Marshall MV, Sevick-Muraca EM. New horizons for imaging lymphatic function. Ann. N.Y. Acad. Sci. 2008; 1131:13. [PubMed: 18519956]

Stacker SA, Achen MG, Jussila L, Baldwin ME, Alitalo K. Lymphangiogenesis and cancer metastasis. Nat. Rev. Cancer. 2002; 2:573. [PubMed: 12154350]

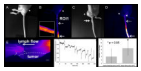

Figure 1.

Abnormal lymphatic drainage pathways and tortuous, dilated collecting lymphatic vessels in tail-tumor-bearing mice. White light (A) and fluorescent (B) images in a tumor-free mouse showing fluorescent lymphatic capillaries (inset) near the injection site (arrow) and collecting lymphatic vessels (broken arrow) draining to the ischial LN (asterisk). *Scale bar*: 1 mm. White light (C) and fluorescent (D) images in a tail-tumor-bearing mouse depicting abnormal lymphatic passage to the abdominal region as denoted by the arrow head. *Arrow*: injection site. *Double arrow*: tumor. (E) Two fluorescent images stitched together in a tail-tumor-bearing mouse showing no uptake of fluorophore in the lymphatic capillaries in the skin above the tumor and tortuous and mispatterned collecting lymphatic vessels (small arrows) draining to the ischial LN. Flow is from right to left (distal to proximal). *Scale bar*: 1 mm. (F) Normalized fluorescent intensities as a function of time in the ROI1 selected on the fluorescent collecting lymphatic vessel shown in Figure 1B. (G) Collecting lymphatic vessels in tail tumor-bearing mice show significantly reduced number of contractions, as compared to those in normal mice. Error bars show the standard deviation.

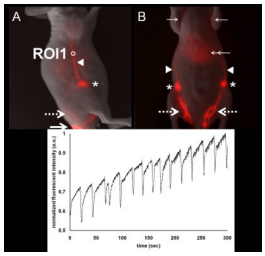

Figure 2.

Normal lymphatic drainage pathways and function in a tumor-free mouse. Overlay of white light and fluorescent images in the right lateral view (A) and the ventral view (B) of a normal mouse showing lymphatic trafficking of ICG-labeled lymph from the injection site (large arrow), through the lymphatic plexus (large broken arrow), to the inguinal LN (asterisk) and subsequently to the axillary LN (small arrow) via the internodal collecting lymphatic vessels (arrow head). (C) Normalized fluorescent intensity as a function of time in ROI 1 selected in a fluorescent internodal collecting lymphatic vessel as shown in Figure 2B illustrates contractile activity and propelled lymph flow. Supplemental Figure 1 shows non-overlaid, pseudo colored fluorescence imaging of (B) showing more clearly the axillary lymph nodes.

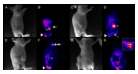

Figure 3.

Abnormal lymphatic drainage and function and leaky lymphatic vessels in hindlimb-tumor-bearing mice. White light (A) and fluorescent (B) images in a mouse without palpable LN involvement at 2 weeks tumor p.i. show abnormal lymphatic drainage pathway (arrow) from the inguinal LN (asterisk). White light (C) and fluorescent (D) images in another mouse with palpable inguinal LN involvement at 2 weeks p.i. represent the enlarged fluorescent inguinal LN (asterisk) and leaky lymphatic vessels as indicated by bright spots (broken arrow). White light (E) and fluorescent (F) images in a mouse with the inguinal and axillary LN metastases showing dilated and tortuous fluorescent lymphatic vessels bypassing the primary tumor and the inguinal (Asterisk) and axillary LNs, and eventually draining to the brachial LN (double arrow). *Arrow head*: injection site. White light (G) and fluorescent (H) images of the ventral view of a tumor-bearing mouse with the massive inguinal and axillary LN metastases represent extensive ICG staining of lymphatic vessels, which are dilated and tortuous. The inset of Figure 3H shows a magnified fluorescent image of the rectangle in Figure 3H depicting diffused dye patterns. *Scale bar*: 1 mm.

Table 1

Summary of the status of lymphatic drainage pattern and LN metastasis in mice (N=10) with a hindlimb tumor

	2wk	3wk
# mice with palpable inguinal LNM	3/10 *(2*/3 had normal drainage; 1/3 had altered drainage)*	9/10 *(2+/9 had normal drainage; 7/9 had normal drainage)*
# mice with palpable inguinal and axillary LNM	0/3	5/9 *(5/9 had altered drainage)*
# mice without palpable inguinal LNM	7/10 *(5**/7 had normal drainage; 2/7 had altered drainage)*	1/10 *(1++/1 had normal drainage)*

Abbreviation: LNM, LN metastasis

* two mice showed no lymphatic contractile function

+ one of two mice showed no contractile function and the other showed 4 pulses

** two of five mice showed no contractile function and the others showed 21, 5, and 3 pulses

++ one mouse showed 36 pulses